Rock Mechanics and Rock Engineering (2019) 52:4619–4635
https://doi.org/10.1007/s00603-019-01846-0

ORIGINAL PAPER

# Role of Tectonic Coal in Coal and Gas Outburst Behavior During Coal Mining

Qingyi Tu[1,2,3] · Yuanping Cheng[1,2] · Ting Ren[3] · Zhenyang Wang[1,2] · Jia Lin[3] · Yang Lei[1,2]

Received: 10 July 2018 / Accepted: 4 May 2019 / Published online: 21 May 2019


## Abstract

Coal and gas outbursts are small-scale geological disasters controlled by tectonic movement, and tectonic coal is widespread in outburst zones. In this study, we compare tectonic and intact coal specimens to examine the basic properties of tectonic coal. We estimate the different energies and limits of the crushing work ratio of coal from five typical outburst cases using on-site outburst data, and discuss the relationship between outbursts and tectonic coal. The results show that tectonic coal is a product of tectonic movement and its original primary structure is destroyed during the tectonic process. Compared with intact coal, tectonic coal shows low strength properties and a crushing work ratio of 22.11 J/m$^2$. The specific surface area and total pore volume of the minipores, mesopores, and macropores of the coal strongly increase under conditions of intense tectonism, which indicates that tectonic coal has a very high capacity for rapid initial gas desorption. An adequate supply of gas is required to transport outburst coal, such that the existence of coal particles smaller than the critical diameter is important. Our calculations indicate that the crushing work ratio of coal from the five outburst case ranges from 22.19 to 78.67 J/m$^2$. Only the crushing work ratio of tectonic coal satisfies the requirement for these cases. Therefore, the properties of the tectonic coal and crushing work ratio for the five cases indicate that the widespread occurrence of tectonic coal plays a crucial role in outbursts.

**Keywords** Coal and gas outburst · Tectonic coal · Tectonic movement · Outburst energy · Crushing work ratio

## List of Symbols

| | |
|---|---|
| $f$ | Protodyakonov coefficient |
| $a$ | Gas adsorption constant |
| $b$ | Gas adsorption constant |
| $M_{ad}$ | Moisture content |
| $A_d$ | Ash content |
| $V_{daf}$ | Volatile content |
| $W$ | Total crushing work |
| $m$ | Mass of the hammer |
| $h$ | Drop height |
| $g$ | Gravitational acceleration |
| $n$ | Impact times |
| $\Gamma$ | Crushing work ratio |
| $\Delta S$ | Newly added surface area |
| $w_{ij}$ | Crushing work of each test |
| $F$ | Applied force |
| $x$ | Displacement |
| $S_i$ | Surface area of the coal particles |
| $G$ | Coal mass |
| $\gamma_i$ | Mass proportion |
| $d$ | Coal particle size |
| $\rho$ | Density of coal |
| $S_0$ | Surface area of initial coal particles |
| $d_m$ | Average particle size of the initial coal particles |
| $W_e$ | Stress energy |
| $W_g$ | Gas energy |
| $W_f$ | Additional energy causing by mining activities |
| $W_1$ | Crushing work |
| $W_2$ | Transport work |
| $W_3$ | Remaining energy |
| $E_e$ | Stress energy per unit volume |
| $\sigma_i$ | Triaxial stresses |
| $E$ | Elastic modulus |

✉ Yuanping Cheng
ypccumt2015@outlook.com

[1] Key Laboratory of Coal Methane and Fire Control, Ministry of Education, China University of Mining and Technology, Xuzhou 221116, China

[2] Faculty of Safety Engineering, China University of Mining and Technology, Xuzhou 221116, China

[3] School of Civil, Mining and Environmental Engineering, University of Wollongong, Wollongong, NSW 2522, Australia

| | |
|---|---|
| $\mu$ | Poisson's ratio |
| $P$ | Gas pressure |
| $V$ | Gas volume |
| $\kappa$ | Adiabatic coefficient |
| $V^{\mathrm{f}}$ | Free gas volume |
| $\phi$ | Coal porosity |
| $V_{\mathrm{m}}$ | Coal volume |
| $D$ | Diffusion coefficient |
| $t$ | Diffusion time |
| $Q_{\mathrm{t}}$ | Gas desorption volume at time $t$ |
| $Q_{\infty}$ | Final gas desorption volume |
| $P_{\mathrm{a}}$ | Atmospheric pressure |
| $V^{\mathrm{a}}$ | Adsorbed gas volume |
| $Q_{it}$ | Gas desorption volume in the $i$ particle-size range |
| $W_{2i}$ | Transport work of the $i$ segment |
| $m_i$ | Outburst coal mass of the $i$ segment |
| $l_i$ | Distance from the outburst point |
| $f_{\mathrm{m}}$ | Friction coefficient |
| $\theta$ | Coal seam angle |
| $v$ | Initial gas desorption rate of coal particles |
| $\zeta$ | Correction factor |
| $\eta$ | The ratio of the average horizontal principal stress to the vertical stress |
| $H$ | Cover depth |
| $\sigma_{\mathrm{H}}$ | Maximum horizontal principal stress |
| $\sigma_{\mathrm{h}}$ | Minimum horizontal principal stress |
| $\sigma_{\mathrm{V}}$ | Vertical stress |
| $\bar{\gamma}$ | Average density of the overlying strata |

## 1 Introduction

Coal is a solid combustible organic rock that is transformed from plant debris via complex processes over a long geological timeframe (Schweinfurth 2003). In addition to sedimentary factors, the coal seams are subjected to complex tectonic action during later period, resulting in complex and diverse structural features (Draper and Boreham 2006). Tectonic processes (e.g., faulting, folding, and slipping) can introduce tectonic stress, which destroys the primary structure of the coal and leads to severe crushing or even pulverization (Shepherd et al. 1981; Yan et al. 2012). Severely crushed or pulverized coal is commonly termed tectonic coal or tectonically deformed coal. In contrast, intact coal has not been affected or has been less affected by tectonic processes and maintains its primary structure.

Coal and gas outburst (hereafter referred to as outburst) is unexpected disaster in underground mines and involves the instantaneous release of gas and stress energies under the combined action of geological factors and mining activities (Chen et al. 2013; Lin et al. 2018). Over the years, many scholars have conducted extensive studies on outburst processes and mechanisms based on on-site investigations, similar experimental simulations and theoretical analyses (Liu et al. 2019; Paterson 1986; Tu et al. 2018b; Xu et al. 2006; Yin et al. 2016). However, several factors (stress, gas, coal properties, geological condition, etc.) affect this type of hazard, and there are complex coupling relationships between these factors (Valliappan and Zhang 1999; Wold et al. 2008; Xue et al. 2014); thus, the mechanisms of outbursts under various geological and mining conditions have not been fully understood (Li et al. 2017; Tu et al. 2016). Currently, the commonly accepted view is comprehensive hypothesis, which is that outbursts are the comprehensive result of stress, gas, and coal properties (Chen 2011; Hanes et al. 1983; Jiang et al. 2015; Xu et al. 2006), and the whole process of an outburst can be divided into four stages, including preparation, trigger, development, and termination (Tu et al. 2018a; Zhao et al. 2016). Nevertheless, most of studies on comprehensive hypothesis only focus on the contributions of stress and gas to outbursts and lack attention to the influence of coal properties on outbursts.

However, studies on outburst cases have proven that tectonic coals are known to be the major causes of coal and gas outburst (Shepherd et al. 1981). Hodot (1966) found that the structural damage coefficient for outburst risk coal seams (in the central zone in Donbass of the Soviet Union) was three times greater than that for no outburst risk coal seams, and large amounts of tectonic coal were found in outburst risk coal seams. Based on a study on relevant literature and outburst sites, Shepherd et al. (1981) confirmed that geological tectonics have been identified as a prime factor in the occurrence of outbursts. Outburst zones usually consist of tectonic coal, and the microscopic structure of this type of coal is quite different from that of intact coal. Sato and Fujii (1989) noted that the area of the outburst zone was approximately 400 $m^2$ and extended upward along the normal fault, which suggested that the normal fault played a great role in the outburst of the Sunagawa coal mine in Japan. Lei et al. (2010) applied the theories of plate tectonics and regional structural evolution to investigate the low indicators (e.g., low gas-bearing capacity and low gas pressure) of outburst mechanisms for the "three soft" coal seam in western Henan, and concluded that serious outbursts in this mining area are controlled by tectonic coal and gas. In addition, Cao et al. (2001) believed that there were three principal factors controlling outbursts associated with reverse faults, and outbursts always occurred within a zone of tectonic coal surrounding the fault. Therefore, these studies confirm that outbursts are miniature geological disasters controlled by tectonic movement, and tectonic coal exists commonly in outburst zones. However, these studies have not conducted an in-depth analysis on the basic properties of tectonic coal; therefore, they have been unable to explain why this kind of coal is prone to outbursts.

In this work, we conducted a series of experiments to compare tectonic and intact coals and study the basic properties of tectonic coal. Using on-site outburst data, we estimate the energies and limits of the crushing work ratio of coal for five typical outburst cases. Additional outburst cases were analyzed to confirm the widespread existence of tectonic coal in outburst zones, and the relationship between outbursts and tectonic coal is discussed in detail.

## 2 Geological Origin of Tectonic Coal

Tectonic coal forms when intact coal is subjected to one or multiple tectonic movements. During the coal-forming process, the primary structure of the coal undergoes brittle fracturing, crushing, ductile deformation, or superposition failure, which may lead to changes in its internal chemical composition and structure (Ju et al. 2005; Li et al. 2011, 2013). On-site investigations (Bustin 1982; Fowler and Gayer 1999; Lei et al. 2010; Lu et al. 2015; Shepherd et al. 1981) have found that tectonic coal is widely distributed across many typical coalfields in three different distribution patterns: regional distribution, local distribution, and stratified distribution.

We use data from the Guhanshan coal mine, located in the Jiaozuo coalfield in Henan Province, China. The Guhanshan mine lies between the Guhanshan fault and Youfang fault (Fig. 1). The tectonic setting is simple: a gently dipping monoclinal structure with an SE strike and NW dip. However, the Jiaozuo coalfield is located in the transition zone between the Taihang orogenic belt and North China tectonic belt. After the coal-forming period (Carboniferous–Permian), the coal strata experienced successive tectonic episodes, including the Indosinian, Yanshanian, Sichuan, and North China movements. The tectonic movement created compressional stress that led to sliding of the $2_1$ coal seam bed in the Guhanshan mine; thus forming tectonic coal. The tectonic coal in seam $2_1$ is stratified, about 1-m thick, and located at the bottom of the coal seam (Fig. 1).

The difference between the tectonic coal and overlying intact coal is shown in Fig. 2. The intact coal is mostly complete with clear surface fractures, and more edges and corners than the tectonic coal. The high strength of the intact coal indicates that it is not easy to break. After the intact coal is broken by a hammer, the fracture extends mainly along the primary weakness plane, and the coal specimen breaks into several irregular-shaped pieces, which are large and lumpy (Fig. 2a). The tectonic coal, however, is similar to reconstructed coal; it shows low strength, which is highly crushed by mining activities, and specimens are easily broken into particles or pulverized by hand, as shown in Fig. 2b.

The distribution of tectonic coal depends on complex geological processes (Alpern 1970; Li et al. 2013). Bedding plane sliding is the main factor controlling the regional distribution and stratified distribution of tectonic coal (Li 2001); these are mostly caused by folds (Fig. 3a) and bedding faults (Fig. 3b). The rheology of coal seams and ductile shear zones caused by bed sliding can also determine whether the deformation is strong or weak, which leads to different coal seam deformation structures.

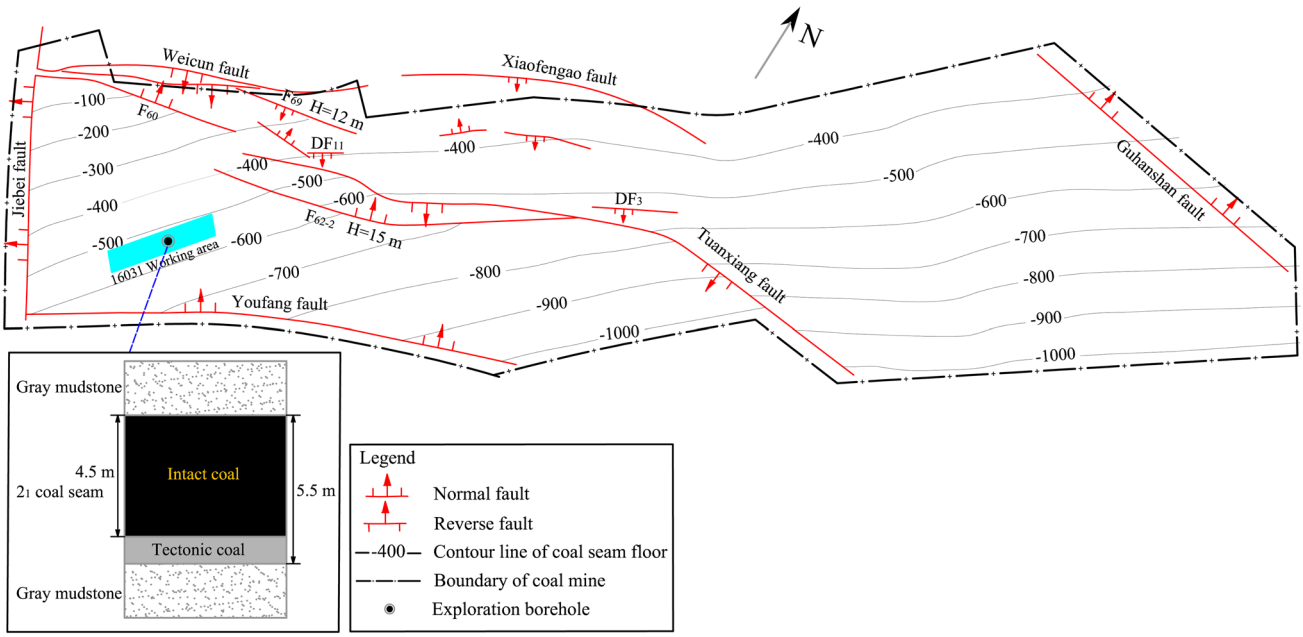


**Fig. 1** Regional geological tectonics and characteristics of the $2_1$ coal seam in the Guhanshan mine

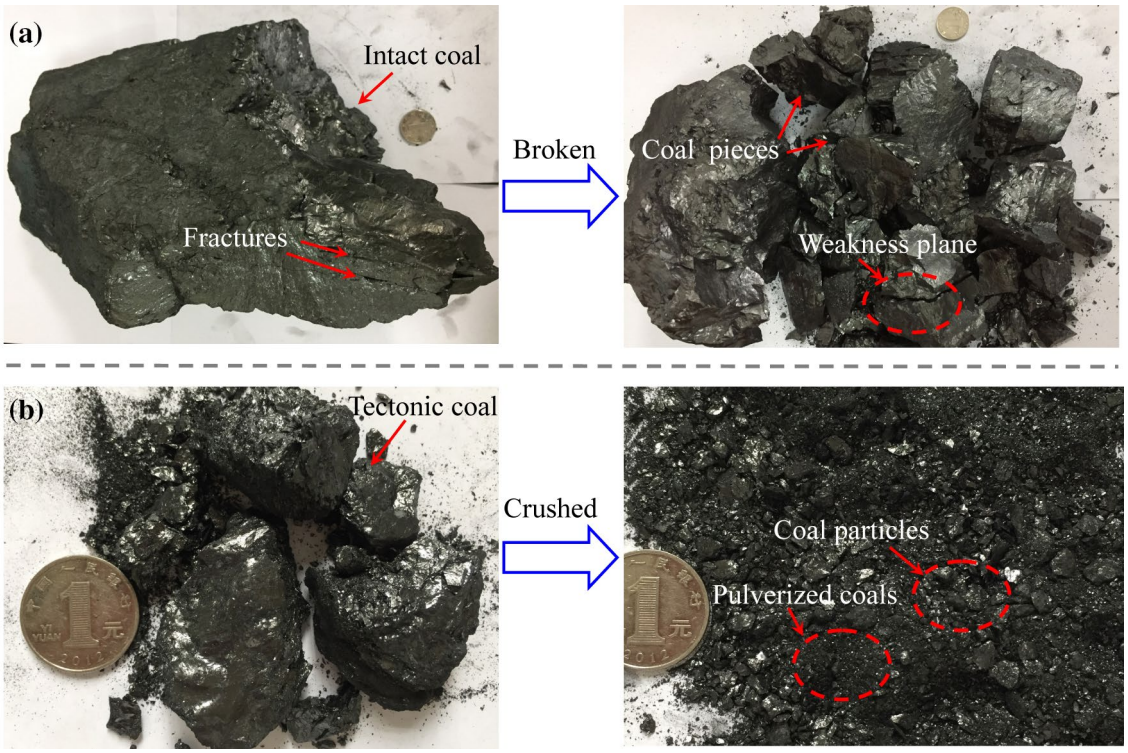


**Fig. 2** Comparison of intact coal with tectonic coal. **a** Intact coal; **b** tectonic coal

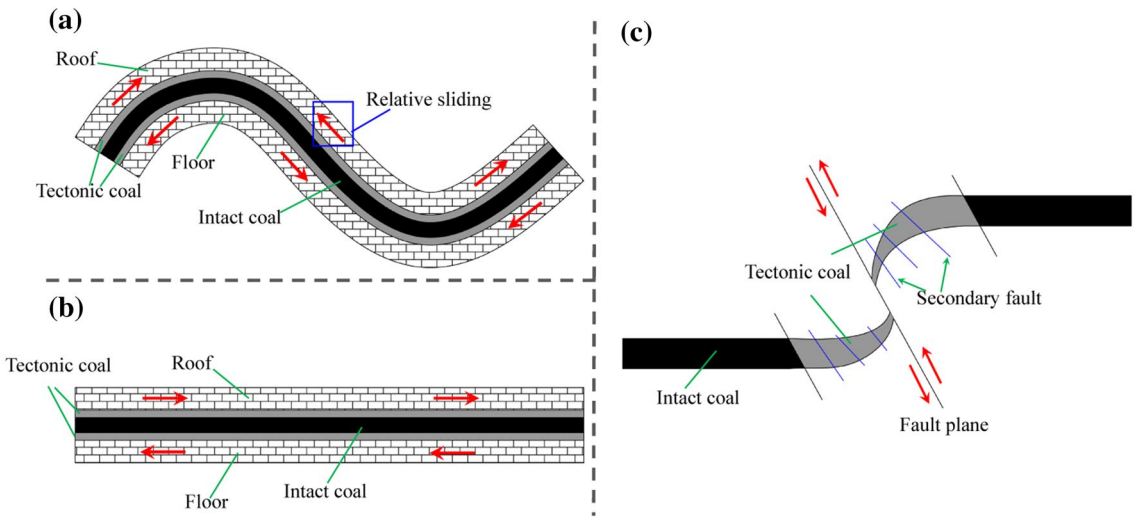


**Fig. 3** Relation between tectonic movements and distribution types of tectonic coals. **a** Fold, **b** bedding fault, and **c** cutting fault

The local distribution is mostly caused by faults cutting through the coal seam in the vertical plane (cutting fault) (Cao et al. 2001), as shown in Fig. 3c. The upper and lower plates of these faults repeatedly interact with each other throughout the geological process, which causes cracking and crushing of the coal, and secondary faults, which develop from the main fault, lead to further destruction.

Ultimately, a fault fracture zone forms near the fault surface where tectonic coal is usually found.

## 3 Tectonic Coal Properties

A series of experiments were conducted to compare tectonic and intact coals. These tectonic coals and intact coals were collected from the $2_1$ coal seam at the Guhanshan coal mine in Henan Province, China. Meanwhile, both tectonic coals and intact coals are collected from the same location (16,031 working area). Prior to the mechanical experiments, the basic parameters of tectonic coal and intact coal were tested. Among them, the basic parameters of tectonic coal are as follows: gas adsorption constants $a = 37.03\,m^3/t$ and $b = 0.85\,MPa^{-1}$; moisture content $M_{ad} = 1.57\%$; ash content $A_d = 13.52\%$; volatile content $V_{daf} = 10.27\%$; and Protodyakonov coefficient $f = 0.18$. In contrast, basic parameters of intact coal are: gas adsorption constants $a = 40.68\,m^3/t$ and $b = 0.71\,MPa^{-1}$; moisture content $M_{ad} = 1.12\%$; ash content $A_d = 13.41\%$; volatile content $V_{daf} = 12.88\%$; and Protodyakonov coefficient $f = 1.50$.

### 3.1 Mechanical Properties

On-site investigations have shown that tectonic coal is highly crushed after mining activities. A complete drill core specimen (e.g., $\Phi 50 \times 100$ mm) of tectonic coal is, therefore, practically impossible to obtain for sample analysis methods routinely applied in intact coal studies (Viete and Ranjith 2006). Hence, we use reconstituted coal specimens as an analog for tectonic coal in a series of mechanical experiments (Liu et al. 2017). To best represent its structural characteristics, tectonic coal with its original particle-size distribution was compressed into a specimen of the desired dimensions ($\Phi 50 \times 100$ mm) using a mold at 100 MPa.

Figure 4 shows the stress–strain curves for tectonic and intact coal under different confining pressures. The tectonic coal (Fig. 4a) undergoes elastic and plastic deformation before reaching peak stress with an axial strain generally $> 2\%$, while plastic deformation of the intact coal (Fig. 4b) is not observed prior to the peak stress. The strength of the tectonic coal decreases gradually after peak stress, while that of the intact coal decreases more abruptly. The tectonic coal expands upon failure and no macroscopic fractures on the specimen surface were observed. In this state, samples are easily crushed into a larger number of pulverized coal particles (Fig. 4a). In contrast, intact coal undergoes shear failure, the specimens demonstrate clear macroscopic fractures along a given shear angle or primary weakness plane and are broken into several pieces (Fig. 4b).

Table 1 lists the strength and deformation parameters of the tectonic and intact coals. The tectonic coal has a lower uniaxial compressive strength (0.735 MPa) than the intact coal (9.815 MPa), as well as substantially lower cohesion (0.73 MPa vs. 5.39 MPa), both of which are mostly related

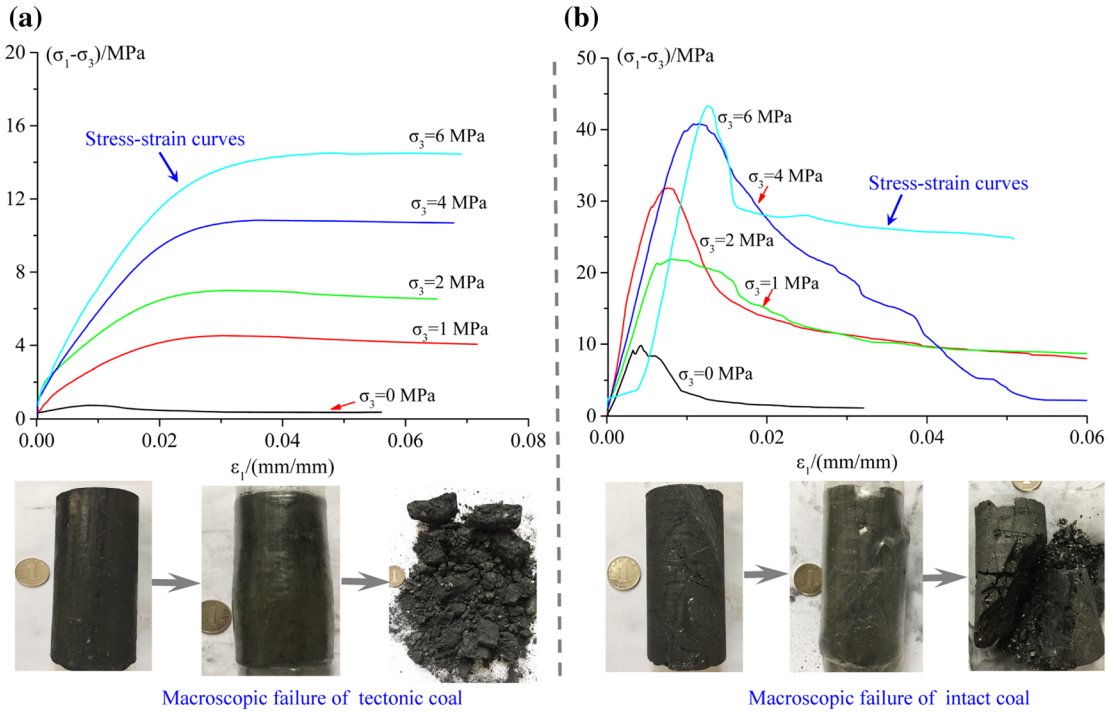


**Fig. 4** Stress–strain curves and macroscopic failure of tectonic and intact coal under different confining pressures. **a** Tectonic coal; **b** intact coal

**Table 1** Strength and deformation parameters of tectonic and intact coals

| Coal | $\sigma_3$ (MPa) | $E$ (MPa) | Poisson's ratio ($\mu$) | $\sigma_{1,\text{peak}}$ (MPa) | $c$ (MPa) | $\theta$ (°) |
|---|---|---|---|---|---|---|
| Tectonic coal | 0 | 168 | 0.39 | 0.735 | 0.73 | 30.0 |
| | 1 | 301 | 0.45 | 5.525 | | |
| | 2 | 485 | 0.27 | 8.99 | | |
| | 4 | 613 | 0.38 | 14.86 | | |
| | 6 | 745 | 0.38 | 20.535 | | |
| Intact coal | 0 | 2700 | 0.37 | 9.815 | 5.39 | 39.0 |
| | 1 | 3520 | 0.48 | 22.875 | | |
| | 2 | 5350 | 0.45 | 33.85 | | |
| | 4 | 4610 | 0.42 | 44.835 | | |
| | 6 | 3650 | 0.37 | 49.33 | | |

to structural differences between the two sample types (Jones et al. 1999). The primary structure of tectonic coal is destroyed by tectonic action and its mechanical properties, which are strongly related to the intraparticle-binding force caused by cementation, are altered. In contrast, the primary structure and mechanical properties of the intact coal remain preserved during deformation.

In addition, the elastic modulus of the tectonic coal increases with confining pressure, but remains several times lower than the intact coal, even though a singularity exists in the intact coal data set.

### 3.2 Pore Structure and Its Effect on Gas Desorption

Coal as a porous medium is a cross-linked macromolecular network structure containing abundant micropores (diameter < 10 nm), minipores (10–100 nm), mesopores (100–1000 nm), and macropores (> 1000 nm) (Cai et al. 2013; Zhang et al. 2017). Coal-forming processes lead to the creation of pores of different sizes and structures, which can be affected by tectonic activity (Ju et al. 2005; Li 2001).

The $N_2$ adsorption and mercury intrusion porosimetry (MIP) methods were used to characterize the pore structures of tectonic and intact coals using a particle size of 5–6 mm (Clarkson and Bustin 1999). Because the reliable measurement range of these two methods is controversial, we employed the $N_2$ adsorption method at 77 K for analyzing coal pores < 300 nm and the MIP method to measure mesopores and macropores > 300 nm (Jin et al. 2018). The Barrett–Joyner–Halenda approach (BJH model) (Barrett et al. 1951) and quenched solid density functional theory (QSDFT model) (Gor et al. 2012) were also applied in the $N_2$ adsorption method. The volume and specific surface area of coal pores were obtained using the QSDFT model for pores < 10 nm and by the BJH model for pores of 10–300 nm in diameter.

The pore size distribution of tectonic and intact coal specimens is presented in Fig. 5. Three peaks are observed in the micropore range of the tectonic coal, while the intact coal shows only a single peak. The tectonic coal pore size distribution curve is higher than the intact coal curve for pores > 10 nm. There are substantial qualitative differences

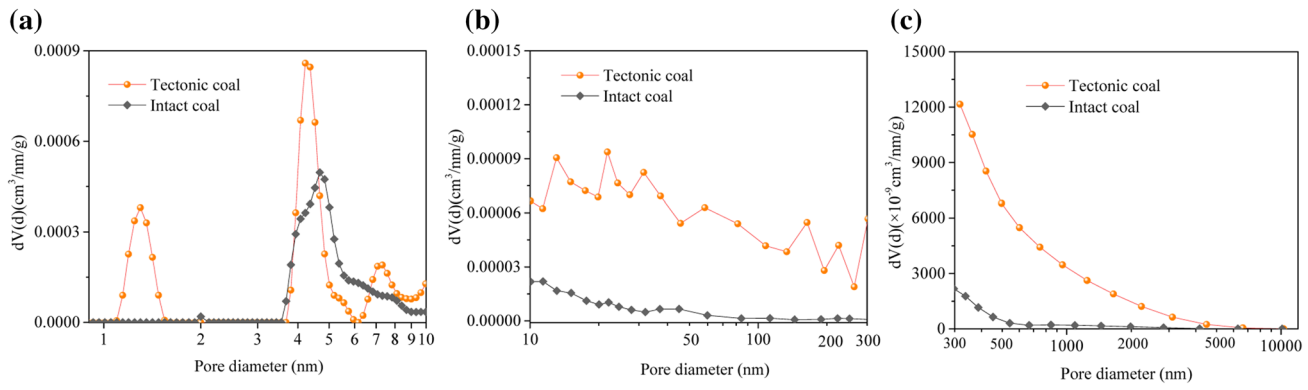


**Fig. 5** Pore size distribution curve of tectonic and intact coals. **a** Pore diameter < 10 nm, **b** pore diameter 10–300 nm, and **c** pore diameter > 300 nm

**Table 2** Comparison of pore volume and specific surface area between tectonic and intact coals

| Parameter | Coal | Pore size distribution | | | |
|---|---|---|---|---|---|
| | | Micropores ($d < 10$ nm) | Minipores ($10 < d < 100$ nm) | Mesopores ($100 < d < 1000$ nm) | Macropores ($d > 1000$ nm) |
| Pore volume ($\times 10^{-3}$ cm$^3$/g) | Tectonic coal | 1.24 | 6.36 | 11.43 | 4.8 |
| | Intact coal | 0.981 | 0.46 | 0.503 | 0.4 |
| Specific surface area (m$^2$/g) | Tectonic coal | 0.988 | 0.64 | 0.1923 | 0.0069 |
| | Intact coal | 0.747 | 0.07 | 0.0059 | 0.00065 |

between the tectonic and intact coals, with sizes ranging from minipores to macropores.

As listed in Table 2, the pore volume and specific surface area of the tectonic coal micropores are $1.24 \times 10^{-3}$ cm$^3$/g and 0.988 m$^2$/g, respectively, which are higher than the intact coal values by a factor of ~ 1.3. The volumes of minipores, mesopores, and macropores, however, are significantly higher in the tectonic coal, by factors of 13.83, 22.72, and 12, respectively, and the specific pore surface areas are 9.14, 32.59, and 10.61 times greater than those of the intact coal, respectively. These results demonstrate that the specific surface area and total pore volume in the larger pores (minipores, mesopores, and macropores) strongly increase under intense tectonic activity, in agreement with the previous studies (Li et al. 2013; Qu et al. 2010).

Pore structure is the controlling factor for gas storage and migration in coal seams (Busch and Gensterblum 2011), which are directly affected by pore structure changes (Cai et al. 2013; Yao et al. 2008). We conducted 120-min desorption experiments at a constant temperature of 30 °C using tectonic and intact coal particles of 1–3 mm in size. The desorption curves are shown in Fig. 6. The desorption volume of both coal types increases with adsorption equilibrium pressure; however, the desorption volume of tectonic coal is 2.27–4.04 times greater than that of the intact coal under the same gas pressure conditions. The gas desorption curve for the tectonic coal flattens later in the 120-min period, while that of the intact coal continues to slowly rise. The results demonstrate that tectonic coal reaches desorption equilibrium within 120 min, while intact coal requires additional time.

Outbursts generally last only a few to a few tens of seconds, and the Zhongliangshan mine outburst lasted 39 s (Tu et al. 2018a). The gas desorption capacity during the initial gas desorption stage, therefore, has a direct effect on outbursts. To assess the initial gas desorption capacities of tectonic and intact coal, the average desorption speeds during the first 30 s are compared as a function of adsorption equilibrium pressures in Fig. 7. Average gas desorption speeds increase with adsorption equilibrium pressure for both coal types during the first 30 s, with 5.69–9.14 times faster speeds observed in the tectonic coal compared with the intact coal

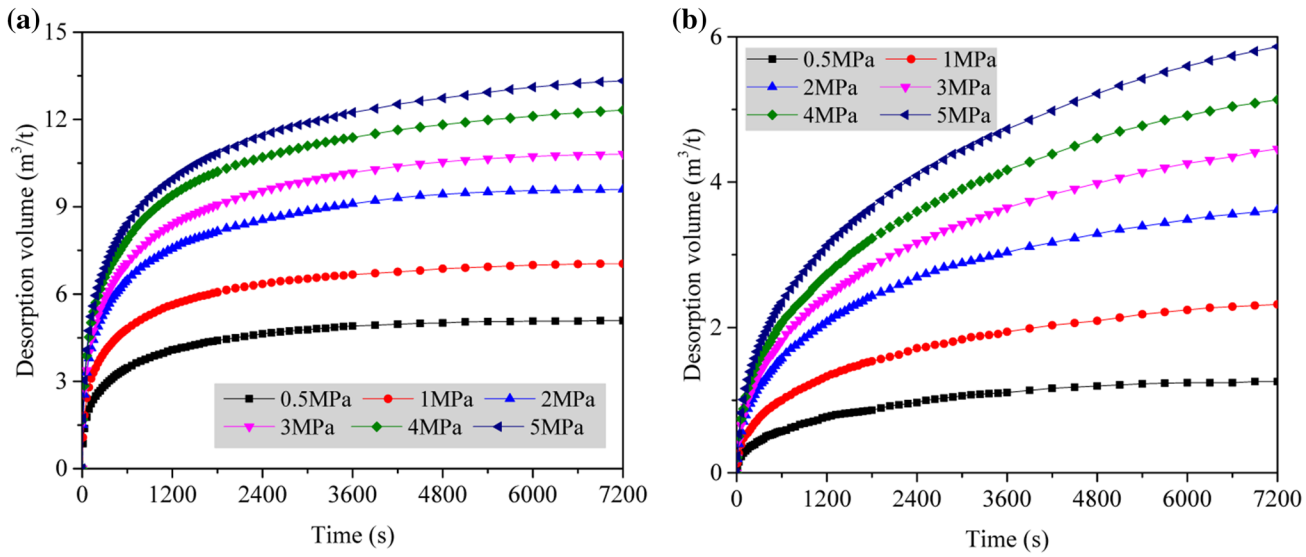


**Fig. 6** Changes in desorption volume over time under different adsorption equilibrium pressure conditions. **a** Tectonic coal; **b** intact coal

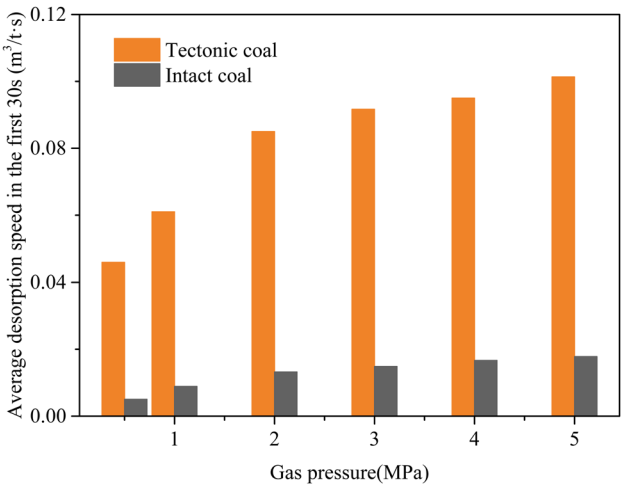


**Fig. 7** Average desorption speeds of tectonic and intact coals in the first 30 s

at the same pressure. This indicates that tectonic coal has an extremely rapid initial gas desorption capacity. The pore structure of tectonic coal, thus, controls its initial gas desorption capacity, making it much more prone to outbursts than intact coal (Tu et al. 2016).

### 3.3 Crushing Work Ratio

The crushing work ratio of coal is an important parameter for characterizing the energy demand for crushing. A limited number of studies in the literature have tested the crushing work ratio of coal, generally by means of the impact crushing method (Cai and Xiong 2005; Hodot 1966). During this test, a mass of lump coal is placed in a ramming cylinder and a hammer is dropped from a certain height to impact the sample several times. The total crushing work is calculated as follows:

$$W = mghn, \tag{1}$$

where $W$ represents the total crushing work, J; $m$ represents the mass of the hammer, kg; $h$ represents the drop height, m; $g$ represents the gravitational acceleration, N/m$^2$; and $n$ represents the times of impact.

The newly added surface area $\Delta S$ is obtained by analyzing the particle-size distribution of the crushed coal. The crushing work ratio $\Gamma$ can be calculated as follows:

$$\Gamma = W/\Delta S, \tag{2}$$

where $\Gamma$ represents the crushing work ratio, J/m$^2$; and $\Delta S$ represents the newly added surface area, m$^2$. Equation (1) shows that the total crushing work is related only to external parameters such as $m$, $h$, and $n$. However, an effective conversion rate for the crushing work using this method is difficult to obtain.

We developed an alternative method for testing the crushing work ratio of coal based on the same measuring principle as the impact crushing method. This approach considers the intrinsic properties of coal and is based on the coal particle compression test (Dong et al. 2018). The test was conducted using a TY8000-A uniaxial testing device (Jiangsu Tianyuan Test Equipment Co., Ltd.), as shown in Fig. 8. The device contains two rigid platens, the upper of which can be moved by a servomotor that drives the screw. The applied force was tested by a BAB-5MT or BAB-50MT load transducer, and the displacement was measured using a photoelectricity displacement coder. A coal particle is first placed on the lower platen and then compressed by lowering the upper platen.

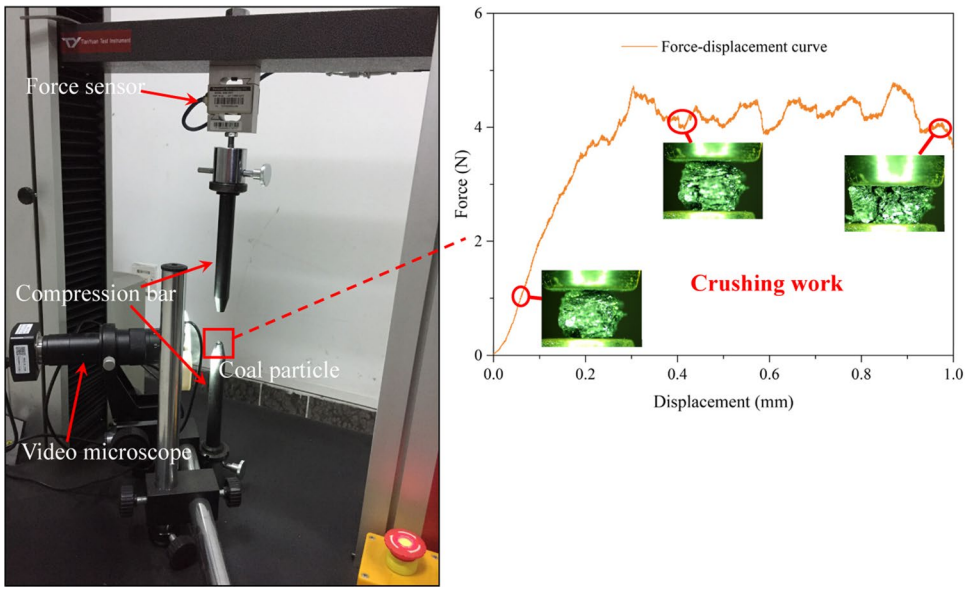


**Fig. 8** Experimental device and force–displacement curve

When the upper platen senses the coal particle by a force of $2\times10^{-3}$ N, the testing system starts to record the loading force and platen displacement. A video microscope is also used to monitor deformation. The force–displacement curve (Fig. 8) derived from the test is integrated to produce the crushing work of the coal particle as follows:

$$w_{ij} = \int_{x_1}^{x_2} F(x)\mathrm{d}x, \tag{3}$$

where $w_{ij}$ represents the crushing work of each experiment, J; $F$ represents the applied force, N; $x$ represents the displacement of the upper platen, m; and $x_1$, and $x_2$ represent the initial and final displacements, respectively (m).

Spherical particles with an intact appearance were selected as the experimental samples. The initial particle sizes of the tectonic and intact coal samples are listed in Table 3. To account for variations between samples, all experiments were repeated and the results were averaged. Eighty particles of both tectonic and intact coal were used, and each particle was compressed three-to-five times to ensure crushing. The crushing work per unit mass was calculated for each coal particle, as shown in Fig. 9. The total crushing work and total coal particle mass were used to calculate the average crushing work per unit mass. The results show that the crushing work per unit mass for intact coal is consistently higher than that for tectonic coal, and the average intact coal value (2240.35 J/kg) is ~ 11.27 times greater than that of tectonic coal.

The total crushing work is obtained by the following equation:

$$W = \sum w_{ij}. \tag{4}$$

Using the standard sieves (i.e., the Taylor system), the crushed tectonic and intact coal samples were sieved to obtain the particle-size distribution, as shown in Table 3. The proportions of tectonic and intact coal particles with particle sizes > 1 mm account for 76.98% and 84.97%, respectively. However, the proportion of coal particles with a particle size < 0.5 mm is higher in the tectonic coal than in the intact coal. Moreover, pulverized coal, with a particle size < 0.075 mm, was found in the tectonic coal but not in the intact coal.

Based on the assumption that the coal particles are spherical before and after crushing, the average particle size was used to represent the coal particle size in each size range. The average particle size > 4 mm was measured using a Vernier caliper and the results were averaged. The average particle size ≤ 0.075 mm was 0.015 mm, which is consistent with experimental results of Cai and Xiong (2005). The mean value of the particle-size range was used to represent the average particle size in the other six ranges

**Table 3** Particle-size distribution for tectonic and intact coal samples before or after the experiments

| Coal | Initial particle size | | Mass distribution in different size range (%) | | | | | | | Total quality (g) |
|---|---|---|---|---|---|---|---|---|---|---|
| | Range | Average | > 4 mm | 2.8–4 mm | 1–2.8 mm | 0.5–1 mm | 0.25–0.5 mm | 0.18–0.25 mm | 0.075–0.18 mm | < 0.075 mm | |
| Intact coal | 3.71–4.75 | 4.35 | 0 | 19.76 | 65.21 | 9.10 | 3.15 | 0.99 | 1.79 | 0 | 2.94 |
| Tectonic coal | 4.83–8.85 | 6.60 | 41.44 | 16.39 | 19.15 | 8.75 | 5.96 | 2.03 | 4.62 | 1.66 | 16.95 |

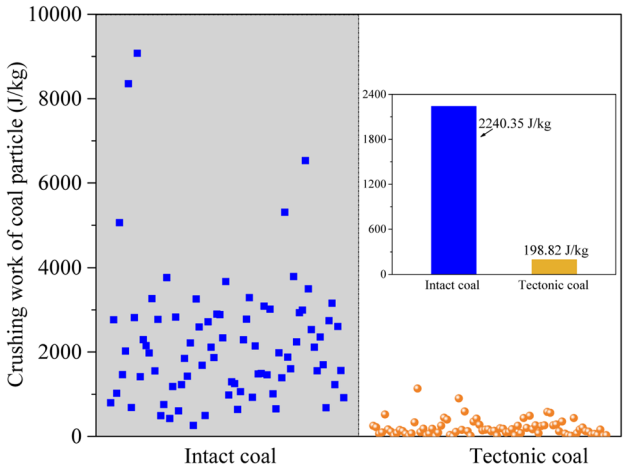


**Fig. 9** Crushing work per unit mass of coal particles

**Table 4** Total crushing work, newly added surface area, and crushing work ratio

| Coal | Total crushing work (J) | Newly added surface area ($m^2$) | Crushing work ratio (J/$m^2$) |
|---|---|---|---|
| Intact coal | 6.4972 | 0.006704 | 969.18 |
| Tectonic coal | 3.0330 | 0.137158 | 22.11 |

from 0.075–0.18 mm to 2.8–4 mm. The surface area of coal particles in the different size ranges can be expressed as follows:

$$S_i = \frac{6G\gamma_i}{\rho d_{im}}, \tag{5}$$

where $S_i$ represents the surface area of the coal particles, $m^2$; $G$ represents the coal mass, kg; $\gamma_i$ represents the mass proportion of coal particles, %; $d_{im}$ represents the average particle size, m; and $\rho$ represents the density of coal, which is considered to be a constant, kg/$m^3$. Thus, the newly added surface area is as follows:

$$\Delta S = \sum S_i - S_0 \tag{6}$$

$$\Delta S = \sum \frac{6G\gamma_i}{\rho d_{im}} - \frac{6G}{\rho d_{\mathrm{m}}}, \tag{7}$$

where $S_0$ represents the surface area of initial coal particles, $m^2$, and $d_{\mathrm{m}}$ represents the average particle size of the initial coal particles, m. Equations (2), (4), and (7) were used to calculate the total crushing work, newly added surface area, and crushing work ratio, respectively. As listed in Table 4, the crushing work ratios for the intact and tectonic coal were 969.18 J/$m^2$ and 22.11 J/$m^2$, respectively. Thus, the crushing work ratio of the intact coal is more than 40 times greater than that of the tectonic coal.

## 4 Outburst Energy Demand of Real Outburst Cases

### 4.1 Outburst Energy

Extensive research conducted by Hodot (1966) and Gale (2018) provides a detailed analysis on outburst energy; the authors noted that outbursts derive their energy from stress energy, gas energy, and additional energy from mining activities. Most of the outburst energy dissipates in the form of work during the outburst process, resulting in the crushing and transport of outburst coal. The remaining energy, which is limited, is transferred into vibration energy and sound energy. This relation is given as follows:

$$W_{\mathrm{e}} + W_{\mathrm{g}} + W_{\mathrm{f}} = W_1 + W_2 + W_3, \tag{8}$$

where $W_{\mathrm{e}}$ represents the stress energy, MJ; $W_{\mathrm{g}}$ represents the gas energy, MJ; $W_{\mathrm{f}}$ represents mining activities with additional energy, MJ; $W_1$ represents the crushing work, MJ; $W_2$ represents the transport work, MJ; and $W_3$ represents the remaining energy, MJ. Mining activities generally play an important role in outburst trigger, but the outburst energy mainly comes from gas energy and stress energy during the outburst development stage. In general, the gas energy and stress energy are much larger than the additional energy from mining activities. Therefore, to simplify the calculations, $W_{\mathrm{f}}$ and $W_3$ are ignored:

$$W_{\mathrm{e}} + W_{\mathrm{g}} = W_1 + W_2. \tag{9}$$

#### 4.1.1 Stress Energy

During the outburst process, the rapid transfer of stress causes the coal to fail, accompanied by the release of stress energy (Feng et al. 2018). Under triaxial stress states, the stress energy of underground coal can be expressed as follows:

$$E_{\mathrm{e}} = \frac{1}{2E}\left[\sigma_1^2 + \sigma_2^2 + \sigma_3^2 - 2\mu\left(\sigma_1\sigma_2 + \sigma_2\sigma_3 + \sigma_3\sigma_1\right)\right], \tag{10}$$

where $E_{\mathrm{e}}$ represents the stress energy per unit volume, MJ/$m^3$; $\sigma_1$, $\sigma_2$ and $\sigma_3$ represent triaxial stresses, MPa; $E$ represents the elastic modulus, MPa; and $\mu$ represents Poisson's ratio. Equation (10) shows that the smaller the elastic modulus, the larger the stress energy.

#### 4.1.2 Gas Energy and Its Source

Gas is one of the outburst power sources and plays an important role in the transport of outburst coal (Sobczyk

2014). Gas contributes to outbursts by the release of expansion energy. However, gas expansion occurring over a short period can be simplified into an adiabatic process:

$$\mathrm{d}W_{\mathrm{g}} = -P\mathrm{d}V, \tag{11}$$

where $P$ represents the gas pressure, MPa, and $V$ represents the gas volume, $m^3$. There is a relationship between gas pressure ($P$) and gas volume ($V$):

$$P_1V_1^{\kappa} = P_2V_2^{\kappa}, \tag{12}$$

where $\kappa$ represents the adiabatic coefficient; $V_1$ represents the gas volume at the gas pressure $P_1$, $m^3$; and $V_2$ represents the gas volume at the gas pressure $P_2$, $m^3$. When the gas pressure changes from $P_1$ to $P_2$, the gas energy is as follows:

$$W_{\mathrm{g}} = \int \mathrm{d}W_{\mathrm{g}} = -\int_{P_1}^{P_2} P\mathrm{d}V = \frac{P_2V_2}{\kappa - 1}\left[\left(\frac{P_1}{P_2}\right)^{\frac{\kappa-1}{\kappa}} - 1\right]. \tag{13}$$

A large amount of gas is required to provide outburst energy. These gases are free and adsorbed gas. Free gas is stored in the fracture system and exists in the gas phase, making it immediately available to participate in the outburst (Zhao et al. 2016):

$$V^{\mathrm{f}} = \phi V_{\mathrm{m}}\left(\frac{P_1}{P_2}\right)^{\frac{1}{\kappa}}, \tag{14}$$

where $V^{\mathrm{f}}$ represents the free gas volume, $m^3$; $\phi$ represents the coal porosity, %; and $V_{\mathrm{m}}$ represents the coal volume, $m^3$. However, the process by which adsorbed gas participates in an outburst is more complex. In essence, adsorbed gas must first desorb and transform into free gas. Assuming that gas desorption on micropore surfaces is an instantaneous process, gas diffusion becomes the factor that controls the involvement of adsorbed gas in the outburst. This process is affected by the particle size and diffusion coefficient (Guo et al. 2016b). Based on the unipore diffusion model (Busch and Gensterblum 2011; Crank 1979), the gas desorption volume of coal particles over a short time can be calculated by the following:

$$\frac{Q_{\mathrm{t}}}{Q_{\infty}} = \frac{12}{\sqrt{\pi}}\left(\frac{D}{d^2}t\right)^{\frac{1}{2}}, \tag{15}$$

where $d$ represents the diameter of a coal particle, m; $D$ is the diffusion coefficient, m/s; $t$ represents the diffusion time, s; $Q_{\mathrm{t}}$ represents the gas desorption volume at time $t$, $m^3$; and $Q_{\infty}$ represents the final gas desorption volume, $m^3$. $Q_{\infty}$ may not change much with coal particle-size variations, because the coal crushing process makes little contribution to the internal pore area. Guo et al. (2014) tested the isothermal adsorption of coal for different particle sizes and obtained several coinciding Langmuir curves:

$$Q_{\infty} = \left(\frac{abP}{1+bP} - \frac{abP_{\mathrm{a}}}{1+bP_{\mathrm{a}}}\right)(1 - M_{\mathrm{ad}} - A_{\mathrm{d}}), \tag{16}$$

where $P_{\mathrm{a}}$ represents the atmospheric pressure, MPa; $M_{\mathrm{ad}}$ represents the moisture content, %; and $A_{\mathrm{d}}$ represents the ash content, %. Therefore, the adsorbed gas volume can be expressed as follows:

$$V^{\mathrm{a}} = \sum Q_{it}, \tag{17}$$

where $V^{\mathrm{a}}$ represents the adsorbed gas volume, $m^3$, and $Q_{it}$ represents the gas desorption volume in the $i$ particle-size range, $m^3$. Based on Eqs. (14) and (17), Eq. (13) can be written as follows:

$$W_{\mathrm{g}} = \frac{P_2}{\kappa - 1}(V_2^{\mathrm{f}} + V_2^{\mathrm{a}})\left[\left(\frac{P_1}{P_2}\right)^{\frac{\kappa-1}{\kappa}} - 1\right]. \tag{18}$$

#### 4.1.3 Dissipation of Outburst Energy

Based on the analysis above, the crushing of coal is one of the necessary processes in an outburst and is important for the quick desorption of adsorbed gas. However, the large amount of newly added surface requires exceedingly high crushing work to overcome the newly added surface energy. Thus, the crushing work can be expressed as follows:

$$W_1 = \Delta S \cdot \Gamma. \tag{19}$$

Assuming only horizontal displacement of coal during the outburst, the transport path of the outburst coal can be divided into several small segments; the transport work in each segment can be expressed by the following:

$$W_{2i} = m_i g(f_{\mathrm{m}}\cos\theta \mp \sin\theta)l_i \times 10^{-6}, \tag{20}$$

where $W_{2i}$ represents the transport work of the $i$ segment, MJ; $m_i$ represents the outburst coal mass of the $i$ segment, kg; $l_i$ represents the distance from the outburst point, m; $f_m$ is the friction coefficient; and $\theta$ represents the coal seam angle, °. Therefore, the total transport work is as follows:

$$W_2 = \sum W_{2i}. \tag{21}$$

### 4.2 Particle-Size Characteristics of Outburst Coal

#### 4.2.1 Particle-Size Distribution of Outburst Coal

According to outburst case studies, the outburst coal is highly crushed or even pulverized with an accumulation angle less than its repose angle. Figure 10a shows the coal particle-size characteristics in the fifth mine of the Yangmei

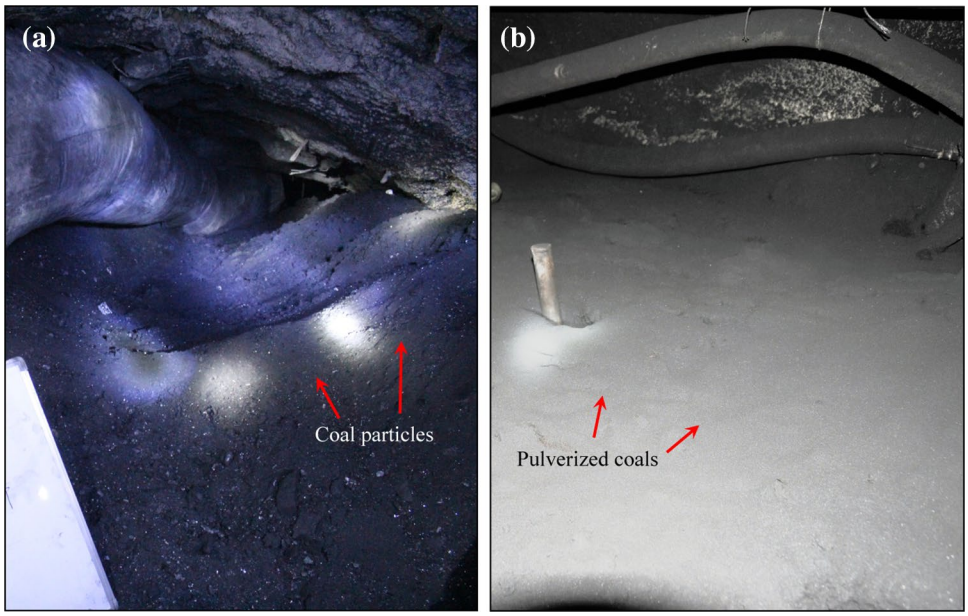


**Fig. 10** Particle-size characteristics of outburst coal. **a** Fifth mine of the Yangmei block outburst and **b** Machang mine outburst

**Table 5** Mass distributions of outburst coals in different particle-size ranges (Hu 2013; Zhao et al. 2016)

| Outburst location | Mass distributions of outburst coal (%) | | | | |
|---|---|---|---|---|---|
| | < 0.1 mm | 0.1–1.0 mm | 1–5 mm | 5–10 mm | > 10 mm |
| # 4 coal seam in Yutianbu mine, + 90-m elevation | 4.6 | 39.1 | 23.5 | 16.0 | 16.8 |
| # 4 coal seam in Yutianbu mine, + 90-m elevation | 3.6 | 38.0 | 31.0 | 17.6 | 9.8 |
| $K_2$ coal seam at the open-off cut of the 5th cross-cut in Zhongliangshan mine, + 280-m elevation | 25.4 | 26 | 27.6 | 1.0 | 20.0 |
| K1 coal seam at the Xisi half rising cross-cut in Zhongliangshan mine, + 280-m elevation | 4.3 | 29.9 | 24.6 | 14.1 | 27.2 |
| K10 coal seam at the 5th cross-cut in Zhongliangshan mine, + 280-m elevation | 3.5 | 30.4 | 30.5 | 19.4 | 16.2 |
| K10 coal seam at the Xisi half rising cross-cut in Zhongliangshan mine, + 280-m elevation | 6.6 | 27.5 | 16.9 | 18.2 | 30.8 |
| # 6 coal seam in Nantong mine, − 100-m elevation | 1.1 | 11.9 | 23.9 | 23.5 | 39.5 |
| Average value | 7.0 | 29.0 | 25.4 | 15.7 | 22.9 |

block outburst, and Fig. 10b shows pulverized coal from the Machang mine outburst.

Hu (2013) investigated coal particle composition in several outburst cases, and the mass distribution of the outburst coal is shown in Table 5. These outburst coals contain a large fraction (> 30%) of ≤ 1.0-mm coal particles, while pulverized coal with particles < 0.1 mm are also found in proportions ranging from 1.1 to 25.4% at the different outburst locations.

### 4.2.2 Role of Pulverized Coal in Rapid Gas Desorption

Assuming that coal is an isotropic material, Zhao et al. (2016) proposed that the diffusion coefficient $D$ does not vary with particle size under the same concentration difference; noting that the initial gas desorption speed ($v$) of coal particles is proportional to the particle size ($d$):

$$\frac{v_1}{v_2} = \frac{d_2}{d_1}, \tag{22}$$

where $v_1$ and $v_2$ represent the initial gas desorption speed of coal particles, with corresponding coal particle sizes of $d_1$ and $d_2$, respectively. By considering the influence of inhomogeneity, Watanabe (1985) obtained a modified relation between $d$ and $v$ as follows:

$$\frac{v_1}{v_2} = \left(\frac{d_2}{d_1}\right)^{\zeta}, \tag{23}$$

where $\zeta$ is the correction factor. Both Eqs. (22) and (23) indicate that a decrease in $d$ causes an increase in $v$ (Guo et al. 2016a). Busch et al. (2004) reported a critical diameter for the desorption of coal particles. Similar results were obtained in studies by Airey (1968), Jin et al. (2016) and Zhao et al. (2016). When the coal particle is larger than the critical diameter, $v$ decreases with increasing $d$. However, when the coal particle is smaller than the critical diameter, $v$ increases sharply as $d$ decreases.

As mentioned above, outburst coal contains a large fraction of coal particles with particle sizes less than the critical diameter. These coal particles generally have the ability to rapidly desorb gas. The existence of these small coal particles leads to the rapid desorption of adsorbed gas within the outburst process, which is a very important gas energy source for outbursts.

### 4.3 Energy Calculation for Real Outburst Cases

Table 6 summarizes five typical outburst cases that occurred in China at depths ranging from 203 to 800 m in shallow-crust regions. According to the classification of outburst coal mass (An and Cheng 2014), the intensity types for these cases include sub-large-scale outbursts (outburst coal mass: 100–499 t), large-scale outbursts (outburst coal mass: 500–999 t), and oversized outbursts (outburst coal mass ≥ 1000 t). Unsurprisingly, all of these outbursts occurred in tectonic zones such as areas containing faulting and folding, particularly synclinal axis areas. The coal seam gas pressure is 1.0–2.0 MPa, and large amounts of highly crushed or pulverized coal are found in these cases.

There are two principal stresses at or near the horizontal plane influenced by gravity and tectonic stress. The maximum horizontal principal stress is generally greater than the vertical stress in shallow crust (Hudson and Cooling 1988; Liu et al. 2014). Brown and Hoek (1978) summarized global in situ stress measurement results and found that the ratio of the average horizontal principal stress to the vertical stress ($\eta$) generally lies within limits defined by the following:

$$\eta = \frac{\sigma_H + \sigma_h}{2\sigma_V} \tag{24}$$

$$\frac{100}{H} + 0.3 \le \frac{\sigma_H + \sigma_h}{2\sigma_V} \le \frac{1500}{H} + 0.5, \tag{25}$$

where $\eta$ represents the ratio of the average horizontal principal stress to the vertical stress; $H$ represents the cover depth, m; $\sigma_H$ represents the maximum horizontal principal stress, MPa; $\sigma_h$ represents the minimum horizontal principal stress, MPa; and $\sigma_V$ represents the vertical stress, MPa. The vertical stress is approximately equal to the gravity of the overlying strata:

$$\sigma_V \approx \bar{\gamma} g H, \tag{26}$$

where $\bar{\gamma}$ represents the average density of the overlying strata, which usually is 2500 kg/m$^3$. In addition, Liu et al. (2014) summarized in situ stress measurement results from the Huainan coalfield at a depth range of 350–1100 m and derived the upper and lower limits of the two horizontal principal stresses. The upper limits are as follows:

$$\begin{cases} \sigma_H = 0.0335H + 4.621 \\ \sigma_h = 0.0201H + 4.116 \end{cases}, \tag{27}$$

and the lower limits are

$$\begin{cases} \sigma_H = 0.0101H + 8.721 \\ \sigma_h = 0.0064H + 3.728 \end{cases}. \tag{28}$$

Hence, Eq. (26) is used to estimate the vertical stresses. Equations (27) and (28) are used to estimate the upper and lower limits of the two horizontal principal stresses, respectively, from which an average value is taken. Thus, the three principal stresses of the five case studies can be estimated, as

**Table 7** Estimation of three principal stresses for five outburst cases

| Outburst case | $\sigma_V$ (MPa) | $\sigma_H$ (MPa) | $\sigma_h$ (MPa) | $\eta$ |
|---|---|---|---|---|
| Daping coal mine | 15.3 | 20.01 | 12.03 | 1.047 |
| Xiangshui coal mine | 5.08 | 11.10 | 6.61 | 1.745 |
| Machang coal mine | 16.75 | 21.28 | 12.80 | 1.017 |
| Bailongshan coal mine | 12.5 | 17.57 | 10.55 | 1.125 |
| Fifth mine of the Yangmei block | 20.0 | 24.11 | 14.52 | 0.966 |

**Table 6** Coal and gas outburst cases

| Outburst case | Date | Cover depth (m) | Gas pressure (MPa) | Outburst coal mass (t) | Outburst distance (m) | Structure |
|---|---|---|---|---|---|---|
| Daping coal mine | 2004/10/20 | 612 | 2.0 | 1894 | 256 | Fault area |
| Xiangshui coal mine | 2012/11/24 | 203 | 1.65 | 490 | 66 | Serious structural area |
| Machang coal mine | 2013/03/12 | 670 | 1.2 | 2051 | 188 | Serious structural area |
| Bailongshan coal mine | 2013/09/01 | 500 | 1.57 | 868 | 200 | Fault area |
| Fifth mine of the Yangmei block | 2014/05/13 | 800 | 1.0 | 325 | 30 | Synclinal axis |

listed in Table 7. Average $\eta$ values for the five case studies are 1.047, 1.745, 1.017, 1.125, and 0.966; all of which lie within the limits defined by Eq. (25). Moreover, most values are within the range of 0.8–1.2, which is common in China (Liu et al. 2014).

As shown in Table 5, the mass distribution of the outburst coal samples in these five cases was also divided into five particle-size ranges: $<0.1$ mm, 0.1–1.0 mm, 1.0–5.0 mm, 5.0–10 mm, and $>10$ mm. The particle size in each size range was characterized by the mean value of the particle-size range, except for the size range $>10$ mm, which was simplified to 10 mm.

The influence of the original surface area on the newly added surface area was limited, and the former was thus ignored. The total newly added surface area of the outburst coal was calculated using Eq. (7). The contributions of coal particles in the different particle-size ranges to the total newly added surface area were obtained, as shown in Fig. 11. The results show that the generation of pulverized coal ($d<0.1$ mm) had the greatest impact on the newly added surface area (68.1%). The proportion of coal particles with particle size $>10$ mm was 22.9%, but these had little effect on the newly added surface area (1.1%).

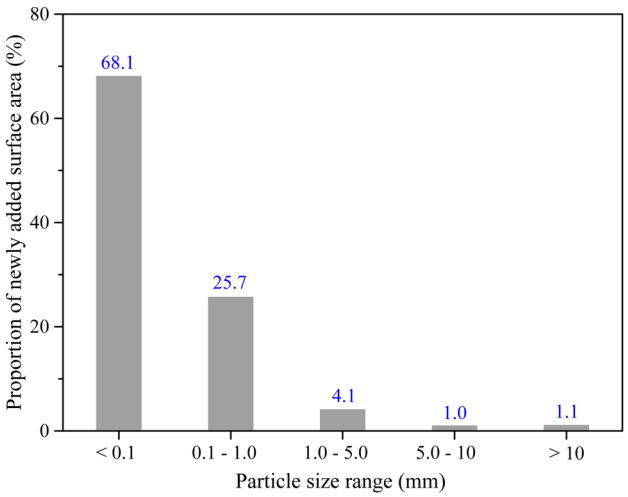


**Fig. 11** Contribution of coal particles in different particle-size ranges to the total newly added surface area

Equations (10), (18), and (21) were used to calculate the stress energy, gas energy, and transport work, respectively, and the crushing work ratio was calculated by Eq. (19). To simplify the calculation, outburst coal was regarded as having a uniform distribution with a friction coefficient $f_m$ of 0.5 (Hodot 1966; Tu et al. 2018a). However, because the data are relatively old and cannot be reproduced, exact descriptions of these outbursts are difficult to obtain. Certain parameters and conditions must be empirically established to obtain a reliable answer, as based on observations or experimental data (Dong et al. 2017; Gercek 2007; Hodot 1966; Jin et al. 2018; Medhurst and Brown 1998; Pan et al. 2013; Tu et al. 2018a). The values of these parameters are: outburst time $t=39$ s; elastic modulus $E=2000$ MPa; Poisson's ratio $\mu=0.32$; coal density $\rho=1.4\times10^3$ kg/m$^3$; porosity $\phi=6\%$; atmospheric pressure $P_a=0.1$ MPa; diffusion coefficient $D=5\times10^{-12}$ m$^2$/s; adiabatic coefficient $\kappa=1.31$; gas adsorption constants $a=35$ m$^3$/t and $b=0.8$ MPa$^{-1}$; moisture content $M_{ad}=1.3\%$; and ash content $A_d=13.5\%$.

Results detailing the different energies involved in the outburst cases are shown in Table 8. It is clear that 662.35–5736.40 m$^3$ (30 °C, 0.1 MPa) of the adsorbed gas is utilized for these cases, which is 7.18–8.61 times greater than that of the free gas. Gas supplies most of the outburst energy, but the contribution of stress energy to the outbursts is also significant, especially for large-scale or oversized outburst.

Based on detailed studies which were conducted by Zhao et al. (2016), adequate gas energy is required for outburst development and the transport of outburst coal. However, a large amount of adsorbed gas is needed for an outburst to occur; therefore, the existence of coal particles with a particle size less than the critical diameter is particularly important to ensure sufficient gas supply.

According to the energy conversion relationship, the stress energy and residual gas energy (except for the depletion of transport work) used for coal crushing are limited. In this situation, the coal must have low strength and cohesion (i.e., easily crushable). The limits of crushing work ratios of the outburst coal for these five cases range from 22.19 to 78.67 J/m$^2$.

**Table 8** Results detailing the different energies involved in the outburst cases

| Outburst case | Outburst gas quantity (m$^3$) | | Stress energy (MJ) | Gas energy (MJ) | Transport work (MJ) | Crushing work ratio (J/m$^2$) |
|---|---|---|---|---|---|---|
| | Free gas | Absorbed gas | | | | |
| Daping coal mine | 799.02 | 5736.40 | 210.69 | 1965.23 | 1212.16 | 57.75 |
| Xiangshui coal mine | 178.48 | 1352.25 | 15.42 | 405.06 | 80.85 | 78.67 |
| Machang coal mine | 548.21 | 4719.04 | 261.87 | 1103.07 | 963.97 | 22.19 |
| Bailongshan coal mine | 304.40 | 2333.90 | 72.13 | 674.46 | 434 | 40.88 |
| Yangquan No. 5 coal mine | 80.77 | 662.35 | 54.98 | 133.90 | 24.36 | 57.45 |

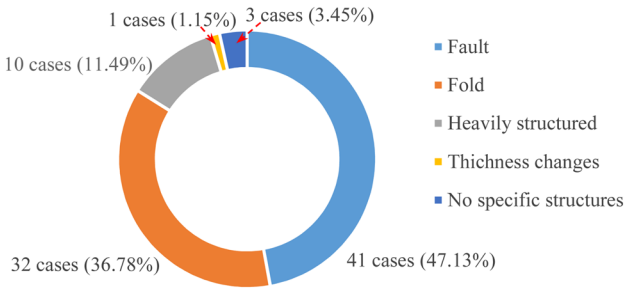


**Fig. 12** The proportion of outbursts that occurred in various tectonic zones

## 5 A crucial Role of Tectonic Coal in Outbursts

Gray (2015) summarized 105 outburst cases from eight coal-producing countries. Among them, 87 outburst cases identified their tectonic type, and 95.4% of these outbursts occurred in tectonic zones (Fig. 12). The specific proportions of outbursts that occurred in faults, folds, and heavily structured zones were 47.13%, 36.78%, and 11.49%, respectively. Only three outburst cases, which occurred in the Bowen Basin of Australia, were found to have no relationship with tectonic action; however, in these three cases, the outburst coal masses were less than 30 t, which were only a few meters long, and their intensities were considerably smaller than those in the other cases. Thus, there exists a qualitatively close relationship between tectonic movement and outbursts, especially for large-scale or oversized outbursts (Wold et al. 2008).

The influence of tectonic movement on outbursts is not only reflected in the change of coal seam stress and gas but also in the destruction of the primary coal structures, which results in the formation of a large amount of tectonic coals in outburst zones (Cao et al. 2001; Wold et al. 2008). Figure 13 shows the Protodyakonov coefficient ($f$) of coal in outburst zones for several cases in China. These $f$ values are very low, with a maximum value of 0.33, indicating that the coal strength in these outburst cases is consistent with that of tectonic coal.

Tectonic coal is extremely prone to outbursts as determined by its properties. Based on the mechanical experiments, both the compressive strength and cohesion of tectonic coal are much less than those for intact coal, the tectonic coal expanded once failure occurred, no macroscopic fractures were observed on the specimen surface, and the specimens were easily crushed into a large number of particles or pulverized particles. In addition, the experiments show that the crushing work ratio of intact coal is 969.18 J/m$^2$, while that of tectonic coal is 22.11 J/m$^2$. The mechanical properties of tectonic coal indicate that it can be crushed easily under low-stress conditions.

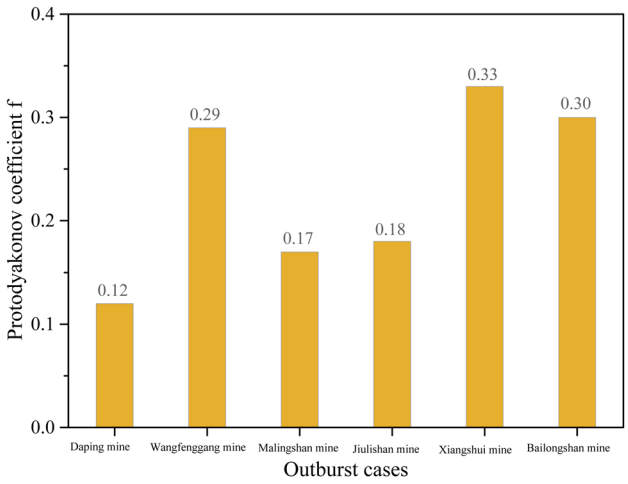


**Fig. 13** The Protodyakonov coefficient ($f$) of coal for outburst cases in China

Complex tectonic movement affects the pore structure of coal. The abundance of larger pores (minipores, mesopores, and macropores) strongly increases under intense tectonic activity, and the volumes and specific surface areas of these larger pores are more than ten times larger in tectonic coal than in intact coal. Pore structure is an important factor that directly affects gas storage and migration in coal seams. Thus, the pore structure of tectonic coal determines its extremely rapid initial gas desorption capacity, which makes tectonic coal much more prone to outbursts compared with intact coal.

Moreover, based on the results detailing the different energies involve in the five outburst cases, an adequate supply of gas is essential for the transport of outburst coal, which is a necessary condition for outburst development. 662.35–5736.40 m$^3$ (30 °C, 0.1 MPa) of the adsorbed gas is utilized for these cases, which is 7.18–8.61 times greater than the energy of the free gas; therefore, the existence of coal particles with particle size less than the critical diameter is particularly important to ensure the gas supply. According to the energy conversion relationship, the stress energy and residual gas energy (except for the depletion of transport work) used for coal crushing are limited. The limits of crushing work ratios of the outburst coal for these five cases range from 22.19 to 78.67 J/m$^2$. It is clear that only the crushing work ratio of tectonic coal satisfies the requirement for these cases.

It can, therefore, be concluded that these pervasive tectonic coals play a crucial role in outbursts.

## 6 Conclusion

Outbursts are small-scale geological disasters controlled by tectonic movement. In this paper, the relationship between outbursts and tectonic coal is discussed, as it is helpful for

recognizing coal and gas outbursts and studying outburst mechanisms. The main conclusions are summarized as follows.

1. Tectonic coal is a product of tectonic movement. Its original primary structure is destroyed during tectonic processes. The crushing work ratio of tectonic coal only is 22.11 J/m$^2$, while the crushing work ratio of the intact coal is tens of times greater than that of the tectonic coal. Compared with intact coal, tectonic coal shows low strength and cohesion properties. Based on mechanical experiments, the tectonic coal expands once failure occurs, no macroscopic fractures are observed on the specimen surface; and the samples are easily crushed into a large number of particles or pulverized particles.
2. The pore structure of coal undergoes changes due to tectonic movement. The abundance of larger pores (minipores, mesopores, and macropores) increases strongly under intense tectonic conditions. The pore volume and specific surface area of pores in tectonic coal are more than ten times greater than those in intact coal. However, due to the control of pore structures on gas storage and migration, tectonic coal has an extremely rapid initial gas desorption capacity, indicating that tectonic coal is prone to outbursts.
3. An adequate supply of gas is a prerequisite for the transport of outburst coal; thus, the existence of coal particles with sizes less than the critical diameter is particularly important. However, the stress energy and residual gas energy used for coal crushing are limited. The limits of crushing work ratios of outburst coal for the five case studies range from 22.19 to 78.67 J/m$^2$. It is clear that only the crushing work ratio of tectonic coal satisfies the requirement for these cases.
4. Tectonic coal plays a crucial role in outbursts, which are determined by tectonic coal's properties and energy limitations of outbursts. Outburst case studies have also verified the widespread existence of tectonic coal.

**Acknowledgements** The authors are grateful for the supported by Outstanding Innovation Scholarship for Doctoral Candidate of "Double First Rate" Construction Disciplines of CUMT. Yueqiang Xing is gratefully acknowledged for his assistance with the language revision. Comments by all of the anonymous reviewers are highly appreciated.

## References

Airey E (1968) Gas emission from broken coal. An experimental and theoretical investigation. Int J Rock Mech Min Sci Geomech Abstr 5:475–494

Alpern B (1970) Tectonics and gas deposit in coalfields a bibliographical study and examples of application. Int J Rock Mech Min Sci Geomech Abstr 7:67–76

An F, Cheng Y (2014) An explanation of large-scale coal and gas outbursts in underground coal mines: the effect of low-permeability zones on abnormally abundant gas. Nat Hazards Earth Syst Sci 14:2125–2132

Barrett EP, Joyner LG, Halenda PP (1951) The determination of pore volume and area distributions in porous substances. I. Computations from nitrogen isotherms. J Am Chem Soc 73:373–380

Brown E, Hoek E (1978) Trends in relationships between measured in situ stresses and depth. Int J Rock Mech Min Sci 15:211–215

Busch A, Gensterblum Y (2011) CBM and $CO_2$-ECBM related sorption processes in coal: a review. Int J Coal Geol 87:49–71

Busch A, Gensterblum Y, Krooss BM, Littke R (2004) Methane and carbon dioxide adsorption–diffusion experiments on coal: upscaling and modeling. Int J Coal Geol 60:151–168

Bustin R (1982) The effect of shearing on the quality of some coals in the southeastern. Can Cordill Can Inst Min Metall Bull 75:76–83

Cai C, Xiong Y (2005) Theoretical and experimental study on crushing energy of outburst-proneness coal. J China Coal Soc 30:63–66

Cai Y, Liu D, Pan Z, Yao Y, Li J, Qiu Y (2013) Pore structure and its impact on CH4 adsorption capacity and flow capability of bituminous and subbituminous coals from Northeast China. Fuel 103:258–268

Cao Y, He D, Glick DC (2001) Coal and gas outbursts in footwalls of reverse faults. Int J Coal Geol 48:47–63

Chen K (2011) A new mechanistic model for prediction of instantaneous coal outbursts—dedicated to the memory of Prof. Daniel D. Joseph. Int J Coal Geol 87:72–79

Chen P, Wang E, Ou J, Li Z, Wei M, Li X (2013) Fractal characteristics of surface crack evolution in the process of gas-containing coal extrusion. Int J Min Sci Technol 23:121–126

Clarkson C, Bustin R (1999) The effect of pore structure and gas pressure upon the transport properties of coal: a laboratory and modeling study. 1. Isotherms and pore volume distributions. Fuel 78:1333–1344

Crank J (1979) The mathematics of diffusion. Oxford University Press, Oxford

Dong J, Cheng Y, Liu Q, Zhang H, Zhang K, Hu B (2017) Apparent and true diffusion coefficients of methane in coal and their relationships with methane desorption capacity. Energy Fuels 31:2643–2651

Dong J, Cheng Y, Hu B, Hao C, Tu Q, Liu Z (2018) Experimental study of the mechanical properties of intact and tectonic coal via compression of a single particle. Powder Technol 325:412–419

Draper J, Boreham C (2006) Geological controls on exploitable coal seam gas distribution in Queensland. APPEA J 46:343–366

Feng J, Wang E, Chen X, Ding H (2018) Energy dissipation rate: an indicator of coal deformation and failure under static and dynamic compressive loads. Int J Min Sci Technol 28:397–406

Fowler P, Gayer R (1999) The association between tectonic deformation, inorganic composition and coal rank in the bituminous coals from the South Wales coalfield, United Kingdom. Int J Coal Geol 42:1–31

Gale WJ (2018) A review of energy associated with coal bursts. Int J Min Sci Technol 28:755–761

Gercek H (2007) Poisson's ratio values for rocks. Int J Rock Mech Min Sci 44:1–13

Gor GY, Thommes M, Cychosz KA, Neimark AV (2012) Quenched solid density functional theory method for characterization of mesoporous carbons by nitrogen adsorption. Carbon 50:1583–1590

Gray I (2015) Outburst risk determination and associated factors. Australian Coal Research Ltd, Brisbane

Guo J, Kang T, Kang J, Zhao G, Huang Z (2014) Effect of the lump size on methane desorption from anthracite. J Nat Gas Sci Eng 20:337–346

Guo H, Cheng Y, Ren T, Wang L, Yuan L, Jiang H, Liu H (2016a) Pulverization characteristics of coal from a strong outburst-prone coal seam and their impact on gas desorption and diffusion properties. J Nat Gas Sci Eng 33:867–878

Guo H, Cheng Y, Yuan L, Wang L, Zhou H (2016b) Unsteady-state diffusion of gas in coals and its relationship with coal pore structure. Energy Fuels 30:7014–7024

Hanes J, Lama R, Shepherd J (1983) Research into the phenomenon of outbursts of coal and gas in some Australian collieries. In: 5th ISRM Congress. International Society for Rock Mechanics

Hodot BB (1966) Outburst of coal and coalbed gas (Chinese Translation). China Coal Industry Press, Beijing

Hu Q (2013) Coal and gas outburst mechanical mechanism. Science Press, Beijing

Hudson J, Cooling C (1988) In situ rock stresses and their measurement in the UK Part I. The current state of knowledge. Int J Rock Mech Min Sci Geomech Abstr 25:363–370

Jiang C, Xu L, Li X, Tang J, Chen Y, Tian S, Liu H (2015) Identification model and indicator of outburst-prone coal seams. Rock Mech Rock Eng 48:409–415

Jin K, Cheng Y, Liu Q, Zhao W, Wang L, Wang F, Wu D (2016) Experimental investigation of pore structure damage in pulverized coal: implications for methane adsorption and diffusion characteristics. Energy Fuels 30:10383–10395

Jin K et al (2018) Experimental investigation on the formation and transport mechanism of outburst coal-gas flow: implications for the role of gas desorption in the development stage of outburst. Int J Coal Geol 194:45–58

Jones J, Pourkashanian M, Rena C, Williams A (1999) Modelling the relationship of coal structure to char porosity. Fuel 78:1737–1744

Ju Y, Jiang B, Hou Q, Wang G, Fang A (2005) Structural evolution of nano-scale pores of tectonic coals in southern North China and its mechanism. Acta Geol Sin 79:269–285

Lei D, Li C, Zhang Z, Zhang Y (2010) Coal and gas outburst mechanism of the "Three Soft" coal seam in western Henan. Min Sci Technol 20:712–717

Li H (2001) Major and minor structural features of a bedding shear zone along a coal seam and related gas outburst, Pingdingshan coalfield, northern China. Int J Coal Geol 47:101–113

Li M, Jiang B, Lin S, Wang J, Ji M, Qu Z (2011) Tectonically deformed coal types and pore structures in Puhe and Shanchahe coal mines in western Guizhou. Min Sci Technol 21:353–357

Li M, Jiang B, Lin S, Lan F, Wang J (2013) Structural controls on coalbed methane reservoirs in Faer coal mine, Southwest China. J Earth Sci 24:437–448

Li H, Feng Z, Zhao D, Duan D (2017) Simulation experiment and acoustic emission study on coal and gas outburst. Rock Mech Rock Eng 50:2193–2205

Lin J, Ren T, Wang G, Booth P, Nemcik J (2018) Experimental investigation of $N_2$ injection to enhance gas drainage in $CO_2$-rich low permeable seam. Fuel 215:665–674

Liu Q, Cheng Y, Yuan L, Tong B, Kong S, Zhang R (2014) CMM capture engineering challenges and characteristics of in situ stress distribution in deep level of Huainan coalfield. J Nat Gas Sci Eng 20:328–336

Liu Q, Cheng Y, Jin K, Tu Q, Zhao W, Zhang R (2017) Effect of confining pressure unloading on strength reduction of soft coal in borehole stability analysis. Environ Earth Sci 76:173

Liu H, Lin B, Mou J, Yang W (2019) Mechanical evolution mechanism of coal and gas outburst. Rock Mech Rock Eng 52:1591–1597

Lu S, Cheng Y, Li W, Wang L (2015) Pore structure and its impact on $CH_4$ adsorption capability and diffusion characteristics of normal and deformed coals from Qinshui Basin. Int J Oil Gas Coal Technol 10:94–114

Medhurst T, Brown E (1998) A study of the mechanical behaviour of coal for pillar design. Int J Rock Mech Min Sci 35:1087–1105

Pan J, Meng Z, Hou Q, Ju Y, Cao Y (2013) Coal strength and Young's modulus related to coal rank, compressional velocity and maceral composition. J Struct Geol 54:129–135

Paterson L (1986) A model for outbursts in coal. Int J Rock Mech Min Sci Geomech Abstr 23:327–332

Qu Z, Wang GG, Jiang B, Rudolph V, Dou X, Li M (2010) Experimental study on the porous structure and compressibility of tectonized coals. Energy Fuels 24:2964–2973

Sato K, Fujii Y (1989) Source mechanism of a large scale gas outburst at Sunagawa coal mine in Japan. Pure Appl Geophys 129:325–343

Schweinfurth SP (2003) Coal-a complex natural resource: an overview of factors affecting coal quality and use in the United States. US Department of the Interior, US Geological Survey, Washington

Shepherd J, Rixon L, Griffiths L (1981) Outbursts and geological structures in coal mines: a review. Int J Rock Mech Min Sci Geomech Abstr 18:267–283

Sobczyk J (2014) A comparison of the influence of adsorbed gases on gas stresses leading to coal and gas outburst. Fuel 115:288–294

Tu Q, Cheng Y, Guo P, Jiang J, Wang L, Zhang R (2016) Experimental study of coal and gas outbursts related to gas-enriched areas. Rock Mech Rock Eng 49:3769–3781

Tu Q et al (2018a) An analysis of the layered failure of coal: new insights into the flow process of outburst coal. Environ Eng Geosci 24:317–331

Tu Q, Cheng Y, Liu Q, Guo P, Wang L, Li W, Jiang J (2018b) Investigation of the formation mechanism of coal spallation through the cross-coupling relations of multiple physical processes. Int J Rock Mech Min Sci 105:133–144

Valliappan S, Zhang W (1999) Role of gas energy during coal outbursts. Int J Numer Meth Eng 44:875–895

Viete D, Ranjith P (2006) The effect of $CO_2$ on the geomechanical and permeability behaviour of brown coal: implications for coal seam $CO_2$ sequestration. Int J Coal Geol 66:204–216

Watanabe E (1985) The initial gas desorption rate as an index of burst of coal and gas: about the parameter of Kt. Saf Coal Mines 5:56–63

Wold M, Connell L, Choi S (2008) The role of spatial variability in coal seam parameters on gas outburst behaviour during coal mining. Int J Coal Geol 75:1–14

Xu T, Tang C, Yang T, Zhu W, Liu J (2006) Numerical investigation of coal and gas outbursts in underground collieries. Int J Rock Mech Min Sci 43:905–919

Xue S, Yuan L, Wang Y, Xie J (2014) Numerical analyses of the major parameters affecting the initiation of outbursts of coal and gas. Rock Mech Rock Eng 47:1505–1510

Yan J, Wang W, Tan Z (2012) Distribution characteristics of gas outburst coal body in Pingdingshan tenth coal mine. Proc Eng 45:329–333

Yao Y, Liu D, Tang D, Tang S, Huang W (2008) Fractal characterization of adsorption-pores of coals from North China: an investigation on CH4 adsorption capacity of coals. Int J Coal Geol 73:27–42

Yin G, Jiang C, Wang J, Xu J, Zhang D, Huang G (2016) A new experimental apparatus for coal and gas outburst simulation. Rock Mech Rock Eng 49:2005–2013

Zhang K, Cheng Y, Li W, Wu D, Liu Z (2017) Influence of supercritical $CO_2$ on pore structure and functional groups of coal: implications for $CO_2$ sequestration. J Nat Gas Sci Eng 40:288–298

Zhao W, Cheng Y, Jiang H, Jin K, Wang H, Wang L (2016) Role of the rapid gas desorption of coal powders in the development stage of outbursts. J Nat Gas Sci Eng 28:491–501